RESEARCH ARTICLE | MARCH 24 2026

Empirical no-go principles for rigid three-point water models: A physically guided manifold of optimality

Special Collection: Festschrift in honor of Christoph Dellago: Exploring Paths and Barriers in Statistical Mechanics

Jefferson Santana Martins ; Raúl Fuentes-Azcatl ; Marcia C. Barbosa

J. Chem. Phys. 164, 124107 (2026)
https://doi.org/10.1063/5.0322846

The Journal of Chemical Physics ARTICLE pubs.aip.org/aip/jcp

Empirical no-go principles for rigid three-point water models: A physically guided manifold of optimality

Cite as: J. Chem. Phys. 164, 124107 (2026); doi: 10.1063/5.0322846
Submitted: 14 January 2026 • Accepted: 12 March 2026 •
Published Online: 24 March 2026

Jefferson Santana Martins,[1,2,a)] Raúl Fuentes-Azcatl,[3] and Marcia C. Barbosa[1,b)]

AFFILIATIONS

[1] Instituto de Física, Universidade Federal do Rio Grande do Sul (UFRGS), Caixa Postal 15051, 91501-970 Porto Alegre, RS, Brazil
[2] Instituto Federal de Educação, Ciência e Tecnologia Sul-rio-grandense (IFSUL), 95910-016 Lajeado, RS, Brazil
[3] Instituto de Física "Luis Rivera Terrazas," Benemérita Universidad Autónoma de Puebla (BUAP), Apdo. Postal J-48, Puebla 72570, Mexico

Note: This paper is part of the Special Topic Festschrift in Honor of Christoph Dellago: Exploring Paths and Barriers in Statistical Mechanics.

[a)] **Electronic mail:** jefferson.santana@gmail.com
[b)] **Author to whom correspondence should be addressed:** marcia.barbosa@ufrgs.br

ABSTRACT

Rigid three-point water models are widely used in molecular simulations, yet they cannot simultaneously reproduce thermodynamic, dielectric, and dynamical properties. We show that these failures do not stem from incomplete parameter optimization, but from physical constraints that define the topology of the model parameter space. Treating the density anomaly as a master thermodynamic constraint, we find that viable geometries and electrostatics collapse onto a low-dimensional physical manifold governed by scaling relations. Within this framework, we identify two topological constraints, an empirical no-go principle, intrinsic to rigid three-point models with standard Lennard-Jones interactions. First, in the small-angle regime ($\theta \lesssim 108^\circ$), matching the experimental dielectric constant requires molecular elongation that destabilizes the hydrogen-bond network and shifts the temperature of maximum density. Second, enforcing the density anomaly increases network rigidity, suppressing molecular mobility, and preventing agreement with the experimental self-diffusion coefficient. Together, these results define the fundamental limits of rigid three-point water models and recast their development as a constrained design problem rather than an empirical optimization task.

I. INTRODUCTION

Liquid water exhibits a set of anomalous thermodynamic and structural properties that continue to challenge molecular modeling. Among these, the temperature of maximum density (TMD) stands out as an exceptionally sensitive probe of the hydrogen-bond network and of the underlying potential energy surface. Even small variations in molecular geometry or electrostatic balance can lead to pronounced shifts—or even disappearance—of this anomaly, making the TMD a stringent benchmark for force-field realism.[1]

Historically, the development of rigid three-point (3P) water models has been approached as a high-dimensional optimization problem, in which electrostatic charges and Lennard-Jones parameters are iteratively adjusted to reproduce selected target properties. This strategy has led to increasingly refined parameterizations, such as TIP3P-FB and OPC3.[2,3] Despite these advances, persistent trade-offs remain: improvements in dielectric response and molecular mobility are frequently accompanied by severe degradation of thermodynamic anomalies, while models that reproduce the density anomaly tend to exhibit systematically suppressed dynamics.[2,3]

It is important to note that empirical manifestations of these limitations have been previously reported. Several studies have documented the persistent difficulty of simultaneously reproducing dielectric, dynamic, and volumetric properties within rigid three-point models.[4–6] However, these studies framed the problem as a

challenge of parameter optimization or force-field design. Here, we demonstrate that these failures originate from intrinsic topological constraints imposed by the density anomaly, elevating these observations to formal no-go conditions.

In this work, we argue that the density anomaly should be elevated from a fitting target to a *master thermodynamic constraint* that fundamentally reorganizes the parameter space of rigid three-point models. In our previous study,[1] we introduced a hierarchical parameterization paradigm demonstrating that the partial charge is the key control parameter governing the existence of the density anomaly. Remarkably, the optimal charge required to reproduce the isobaric density curve was shown to be nearly independent of the H–O–H bond angle, substantially reducing the effective dimensionality of the parameter space. This strategy enabled the construction of models that resolved the long-standing deficiencies of state-of-the-art parameterizations—most notably the large errors in the thermal expansion coefficient—by faithfully capturing the TMD and the volumetric response of the liquid. However, in that previous work, we fixed parameters such as the O–H bond length and a certain range of H–O–H angles.

In this context, here we generalize these insights into a comprehensive diagnostic framework by systematically exploring the geometric degrees of freedom of the O–H length and H–O–H angle and identifying the complete manifold of TMD-consistent models. Within this low-dimensional *physical manifold*, admissible combinations of molecular geometry and electrostatics are no longer freely selectable, but are deterministically coupled by the requirement of reproducing the density anomaly. The development of a water model is, therefore, transformed from an unconstrained optimization problem into one of navigation along physically admissible manifolds.

The central objective of this paper is to use this manifold as a diagnostic tool to delineate the fundamental limits of the rigid three-point architecture through two distinct *no-go conditions*. The first is a geometric–electrostatic incompatibility: for bond angles in the water-like regime (104.5°–106°), reproducing the static dielectric constant requires a degree of molecular elongation that inevitably shifts the temperature of maximum density away from its experimental value. The second is a thermodynamic–dynamic limitation: enforcing the density anomaly necessarily strengthens the hydrogen-bond network, suppressing molecular mobility, and rendering the experimental self-diffusion coefficient unattainable within this model class.

By explicitly mapping this "manifold of optimality," we provide a unified physical explanation for the trade-offs widely reported in the literature. More broadly, this analysis establishes that the long-standing search for a universally accurate rigid three-point water model is fundamentally constrained by topology rather than by a parameterization strategy, thereby defining the ultimate limits of accuracy achievable within this class of models.

II. METHODOLOGY

A. Model definition and interaction potential

In this work, we employ a rigid three-site representation of the water molecule. The molecular geometry is defined by two hydrogen atoms and one oxygen atom constrained to a fixed isosceles triangle configuration, characterized by the length of the OH bond, denoted l, and the angle of the OH bond, θ.

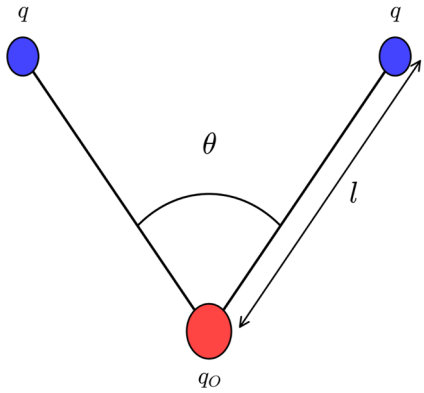

FIG. 1. Schematic representation of the rigid three-site water model employed in this work. The geometry is governed by the bond length l and the bond angle θ. The interaction sites consist of a Lennard-Jones center located at the oxygen atom (characterized by σ_{LJ} and ε_{LJ}) and point charges q_O and q distributed on the oxygen and hydrogen atoms, respectively.

The intermolecular interaction energy U_{ab} between two water molecules a and b is modeled as a superposition of a Lennard-Jones (LJ) potential acting between the oxygen sites and a Coulombic potential acting between all charged sites,

$$U_{ab} = 4\varepsilon_{LJ}\left[\left(\frac{\sigma_{LJ}}{r_{OO}}\right)^{12} - \left(\frac{\sigma_{LJ}}{r_{OO}}\right)^{6}\right] + \sum_{i\in a}\sum_{j\in b}\frac{k_e q_i q_j}{r_{ij}}, \qquad (1)$$

where r_{OO} is the distance between the oxygen atoms of molecules a and b, and ε_{LJ} and σ_{LJ} are the Lennard-Jones potential well depth and the collision diameter (intermolecular distance where the potential is zero), respectively. The second term represents the electrostatic interaction, where k_e is the Coulomb constant, q_i and q_j are the partial charges on the sites i and j, respectively, and r_{ij} is the distance between them. The electrostatic distribution is modeled by placing positive partial charges $+q$ on each hydrogen atom and a compensating negative charge $q_O = -2q$ on the oxygen atom to ensure molecular neutrality. In our parameterization protocol, the dispersive parameter ε_{LJ} is kept fixed, while the geometric parameters (l, θ), the exclusion diameter (σ_{LJ}), and the partial charges (q) are treated as variables to map the manifold of optimality (Fig. 1).

B. Evolution of parameterization strategies

Rigid water models are generally classified by the number of interaction sites, ranging from the computationally efficient three-point (3P) models to the more structurally detailed four- and five-point representations.[7,8] Despite the superior structural accuracy of multi-site models, rigid 3P models remain the workhorses of biomolecular simulation due to their low computational cost. The development of these models has historically followed two distinct paradigms.

The first generation, or "classical models," relied on fixed geometries derived from physical phases. The SPC and SPC/E

models[9,10] adopted the tetrahedral angle of ice ($\theta = 109.47°$), prioritizing the reproduction of bulk density and enthalpy. Conversely, the TIP3P model[11] employed the experimental gas-phase geometry ($\theta = 104.52°$), which, while realistic for a single molecule, necessitated a compromise in liquid-state properties, such as the underestimation of the structure beyond the first coordination shell.

The second generation, or "*modern models*," shifted the focus from physical intuition to mathematical optimization. Approaches such as ForceBalance, used for TIP3P-FB,[2] frame parameterization as a high-dimensional optimization problem, minimizing a penalty function against a broad set of experimental data. Similarly, the OPC3 model[3] was developed through a systematic, exhaustive search of the parameter space to minimize the error in fluid properties. Other strategies, such as the one employed for H2ODC,[4] use sequential optimization of density and dielectric permittivity.

Rigid water models have historically followed divergent developmental paths. The first generation, or "classical models," relied on fixed geometries derived from physical phases. The SPC and SPC/E models[9,10] adopted the tetrahedral angle of ice ($\theta = 109.47°$), prioritizing bulk density and enthalpy. Conversely, the TIP3P model[11] employed the experimental gas-phase geometry ($\theta = 104.52°$), which necessitated a compromise in the liquid-state structure.

The second generation shifted focus from physical intuition to mathematical optimization. Approaches such as ForceBalance (used for TIP3P-FB[2]) and the systematic search of OPC3[3] frame parameterization as a high-dimensional minimization problem against large datasets. While these models successfully reproduce transport and dielectric properties, they often do so by neglecting the physical coupling between parameters, leading to severe degradations in thermodynamic anomalies and interfacial properties.

More recently, distinct efforts have been made to reclaim structural accuracy by prioritizing physical constraints over broad statistical fitting. The TIP3P-ST model,[6] for instance, was explicitly parameterized to reproduce surface tension and density; yet, consistent with the trade-offs we explore in this work, this improvement in cohesion came at the direct cost of suppressed molecular diffusion. Similarly, in our previous study,[1] we proposed a hierarchical parameterization centered on the density anomaly, demonstrating that the hydrogen partial charge is the primary control parameter for the TMD. However, that study was restricted to fixed geometries, leaving the full interplay between bond angle, bond length, and the physical boundaries of the model unexplored. The persistent inability of these approaches—despite their sophistication—to simultaneously reproduce the full hierarchy of water anomalies suggests that the limitation lies not in the optimization method, but in the intrinsic topology of the model's parameter space. It is this fundamental hypothesis that we explore in this work.

C. Parameterization protocol

Our parameterization strategy employs a hierarchical, physically guided approach designed to map the manifold of optimality. The protocol proceeds by decoupling the electrostatic parameter (q) from the steric parameter (σ_{LJ}) based on the following steps:

1. Charge law definition (universal hypothesis): First, we establish the optimal charge–distance relationship, $q(l)$. Based on our previous work,[1] this scaling law was determined by optimizing the partial charge q to satisfy the density anomaly curvature using a fixed, standard geometry ($\theta = 109.47°$). We then hypothesize that this $q(l)$ relationship is a universal property primarily dependent on bond length and largely independent of the bond angle θ.
2. Geometric sampling: We systematically explored the geometric space by varying l within the range $(0.096, 0.103)$ nm. The H–O–H bond angles (θ) were explicitly chosen to represent key physical and historical benchmarks in water modeling, as well as to verify the continuity of the solution space:
   - $\theta = 104.52°$: The experimental angle of the water molecule in the gas phase.
   - $\theta = 106.00°$: An intermediate value chosen to bridge the gap between the experimental geometry and the optimized TIP3P-FB angle, verifying the smoothness of the manifold.
   - $\theta = 108.15°$: The angle optimized for the TIP3P-FB model,[2] representing flexible/force-balanced parameterizations.
   - $\theta = 109.47°$: The ideal tetrahedral angle, characteristic of the hydrogen bond network in ice and used in the classical SPC/E model.[9]
   - $\theta = 110.2°$: The angle used in our previous study.[1]
3. Automated steric optimization (σ_{LJ}): We test this hypothesis for each fixed geometric tuple (l, θ); we apply the universal charge $q(l)$ derived from step 1. This methodology reduces the complex optimization problem to finding a single unknown: the Lennard-Jones size parameter, σ_{LJ}. This parameter is then optimized to reproduce the experimental density at the Temperature of Maximum Density (TMD). We targeted $\rho_{\mathrm{exp}} = 999.9\ \mathrm{kg/m^3}$ at $T = 280\ \mathrm{K}$.[12]

   The Lennard-Jones well-depth parameter $\varepsilon_{\mathrm{LJ}}$ was held fixed at the SPC/E value of 0.65 kJ/mol to isolate the interplay between electrostatics and steric repulsion.[10] While a comprehensive variation of $\varepsilon_{\mathrm{LJ}}$ is beyond the scope of this work, preliminary sensitivity analyses suggest that varying $\varepsilon_{\mathrm{LJ}}$ primarily shifts the vertical position of the $\sigma_{LJ}(l, \theta)$ manifold without altering its fundamental shape or the linearity of the charge scaling law $q(l)$. Thus, the "manifold of optimality" described here represents a cross section of a larger hyper-surface, yet the scaling principles remain robust.

   Supporting simulations using $\varepsilon_{\mathrm{LJ}} = 0.684$ kJ/mol (OPC3 value) confirm that the $q(l)$ scaling remains linear, with only a modest reduction in slope (≈8%), and the topological structure of the manifold, including the no-go boundaries, is preserved. A full mapping of the $\varepsilon_{\mathrm{LJ}}$-extended hypersurface will be presented in a dedicated follow-up study.
4. Algorithmic convergence: The optimization (step 3) was performed using a custom-developed Python automation agent. This agent employs a secant method algorithm, seeded by an intelligent estimator function derived from previously

converged geometric families. Convergence was defined by a stringent tolerance of $|\rho_{sim} - \rho_{target}| \leq 0.3$ kg/m^3.

D. Simulation details

All Molecular Dynamics (MD) simulations were performed using the GROMACS 2021.4 package. The water molecules were treated as rigid three-site bodies, with bond constraints enforced using the SETTLE algorithm. The equations of motion were integrated using the leap-frog integrator with a time step of 2 fs. Long-range electrostatics were evaluated with the Particle Mesh Ewald (PME) method, employing fourth-order interpolation, a real-space cutoff of 1.0 nm, and a Fourier grid spacing of 0.2 nm. Lennard-Jones interactions were truncated at 1.0 nm, and standard long-range dispersion corrections were included for both energy and pressure.

For each candidate parameterization, the simulations followed a standardized equilibration–production protocol. After energy minimization, systems were equilibrated for 100 ps in the canonical ensemble (NVT) using the V-rescale thermostat with a coupling constant of $\tau_T = 0.1$ ps. This step was followed by 500 ps of isothermal–isobaric equilibration (NPT), in which pressure was maintained at 1 bar using the Parrinello–Rahman barostat (isotropic coupling, $\tau_P = 5.0$ ps, compressibility 4.5×10^{-5}, bar^{-1}). Velocities were not reassigned between stages.

Two categories of production simulations were performed: (i) Short production runs (16 ns), from which the first 2 ns were discarded, were used in the parameter-search stage to evaluate density, thermal expansion, and isothermal compressibility. (ii) Long production runs (100 ns) were carried out for the final, selected parameterization to obtain statistically converged estimates of the static dielectric constant, self-diffusion coefficient, and radial distribution functions. All production trajectories were generated in the NPT ensemble using the Nosé–Hoover thermostat ($\tau_T = 1.0$ ps) and the Parrinello–Rahman barostat with the parameters described above.

The total system size consisted of 458 water molecules in a periodically replicated cubic box, matching the standard configuration for benchmarking three-site water models and ensuring consistency with the reference calculations in the literature.

E. Calculation of properties

Thermodynamic properties were derived from the production trajectories using standard statistical mechanical relations and numerical analysis. The temperature of maximum density (TMD) was determined by performing a series of isobaric simulations ranging from 240 to 340 K. The resulting density–temperature profile, $\rho(T)$, was fitted to a fourth-order polynomial, and the TMD was identified as the global maximum of this function. The thermal expansion coefficient, α_P, was subsequently calculated analytically from the derivative of this polynomial fit according to $\alpha_P = -\rho^{-1}(\partial\rho/\partial T)_P$.

The isobaric heat capacity (C_p) was computed as the derivative of the total enthalpy with respect to temperature, $(\partial H/\partial T)_P$, obtained via linear regression of the enthalpy–temperature data. To account for nuclear quantum effects related to the intermolecular librational modes, which are neglected in rigid classical models, a correction of −14.1 J mol^{-1} K^{-1} was applied to the classical C_p values, following the methodology proposed by Vega *et al.*[13]

The isothermal compressibility (κ_T) was calculated from the volume fluctuations in the NPT ensemble using the following relation:

$$\kappa_T = \frac{\langle V^2\rangle - \langle V\rangle^2}{k_B T \langle V\rangle}, \tag{2}$$

where V is the volume of the simulation box, T is the temperature, and k_B is the Boltzmann constant.

For the transport and dielectric properties computed from the long production runs, the self-diffusion coefficient was calculated from the slope of the mean squared displacement (MSD) via the Einstein relation. To correct for finite-size effects inherent to simulations under Periodic Boundary Conditions (PBCs), which systematically underestimate diffusion due to hydrodynamic self-interactions, we applied the Yeh–Hummer correction,[14]

$$D_0 = D_{PBC} + \frac{k_B T \xi}{6\pi\eta L}, \tag{3}$$

where D_{PBC} is the raw diffusion coefficient obtained from the simulation, D_0 is the corrected value, $\xi = 2.837$ is the dimensionless constant for a cubic lattice, η is the shear viscosity, and L is the length of the simulation box edge.

The static dielectric constant (ε) was derived from the fluctuations of the total dipole moment (M) of the system,

$$\varepsilon = 1 + \frac{\langle M^2\rangle - \langle M\rangle^2}{3\varepsilon_0 V k_B T}, \tag{4}$$

where ε_0 is the vacuum permittivity. The liquid–vapor surface tension (γ) was computed using the mechanical definition based on the pressure tensor components. Starting from an equilibrated cubic liquid configuration, the simulation box was elongated in the z-direction to a total length of 10 nm, creating a slab geometry with two liquid–vapor interfaces perpendicular to the z-axis.

Production runs for surface tension were performed in the canonical ensemble (NVT) for 10 ns. The value of γ was determined from the diagonal components of the pressure tensor (P_{xx}, P_{yy}, P_{zz}) using the following relation:

$$\gamma = \frac{L_z}{2}\left\langle P_{zz} - \frac{P_{xx} + P_{yy}}{2}\right\rangle, \tag{5}$$

where L_z is the length of the simulation box normal to the interface, and the factor of 1/2 accounts for the presence of two interfaces in the periodic system.

III. RESULTS AND DISCUSSION

A. The density-consistent manifold

In our previous work,[1] we proposed that there is an optimum hydrogen partial charge (q) for a specific O–H length and H–O–H angle for obtaining the experimental value of the density anomaly, not for a single temperature but for a range of temperatures. In Fig. 2(a), following the strategy proposed in the previous work,[1] we illustrate how this optimum hydrogen charge relates to the O–H length in a linear way. For each value of the optimum charge q, there

is a Lennard-Jones optimum parameter $\sigma_{LJ}(l,\theta)$. Figure 2(b) shows how $\sigma_{LJ}(l,\theta)$ varies with the O–H distance for different θ, indicating a linear result.

The following two fundamental behaviors define this manifold:

- Universal charge scaling: The partial charge required to reproduce the TMD exhibits a robust linear dependence on bond length (l), described by $q(l) \approx -7.68l + 1.21$ $(R^2 > 0.999)$. Crucially, this relationship is largely independent of the bond angle θ.
- Geometric steric compensation: The Lennard-Jones size parameter (σ_{LJ}) also scales linearly with l, but its slope is modulated by θ, creating a family of compensating trajectories.

Physically, these scaling laws represent a necessary energetic balance. As the bond length l increases, the geometric separation of charge centers naturally tends to amplify the molecular dipole moment $(\mu = 2ql\cos(\theta/2))$. If the partial charge q remained constant, this elongation would excessively strengthen electrostatic cohesion, over-stabilizing the tetrahedral network. Therefore, to maintain the specific enthalpy–entropy balance required for the TMD to occur at ~277 K, the partial charge q must *decrease* linearly. This observed trend acts as a compensatory mechanism to counteract geometric amplification, thereby regulating the effective cohesion of the fluid to prevent structural freezing.

The manifold H_2O/DA described above transforms the parameterization problem: one cannot freely choose parameters. To retain the density anomaly, any choice of geometry (l,θ) dictates a specific, non-negotiable set of electrostatic (μ) and steric (σ) parameters. It is strict adherence to this manifold that ultimately gives rise to the limiting empirical no-go principles discussed below.

B. The dielectric-consistent subset and electrostatic master curve

While the manifold defined in Sec. III A ensures density consistency, reproducing the static dielectric constant (ε) adds a second constraint. Our analysis reveals that within the H_2O/DA manifold, ε scales linearly with bond length l for any fixed angle θ (Fig. 3). This linearity allows us to deterministically identify the unique bond length l_{opt} required to match $\varepsilon_{exp} \approx 78.4$ for each H–O–H angle, as shown in Fig. 3.

We define the collection of these dual-consistent models as the H_2O/DA_ε subset. Unlike trial-and-error parameterizations, this

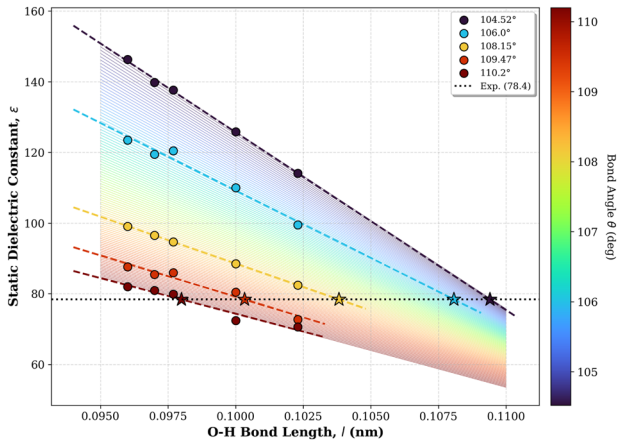

FIG. 3. Universal scaling of ε within the H_2O/DA manifold. The stars indicate the precise intersection with the experimental value $(\varepsilon \approx 78.4)$, defining the members of the H_2O/DA_ε subset.

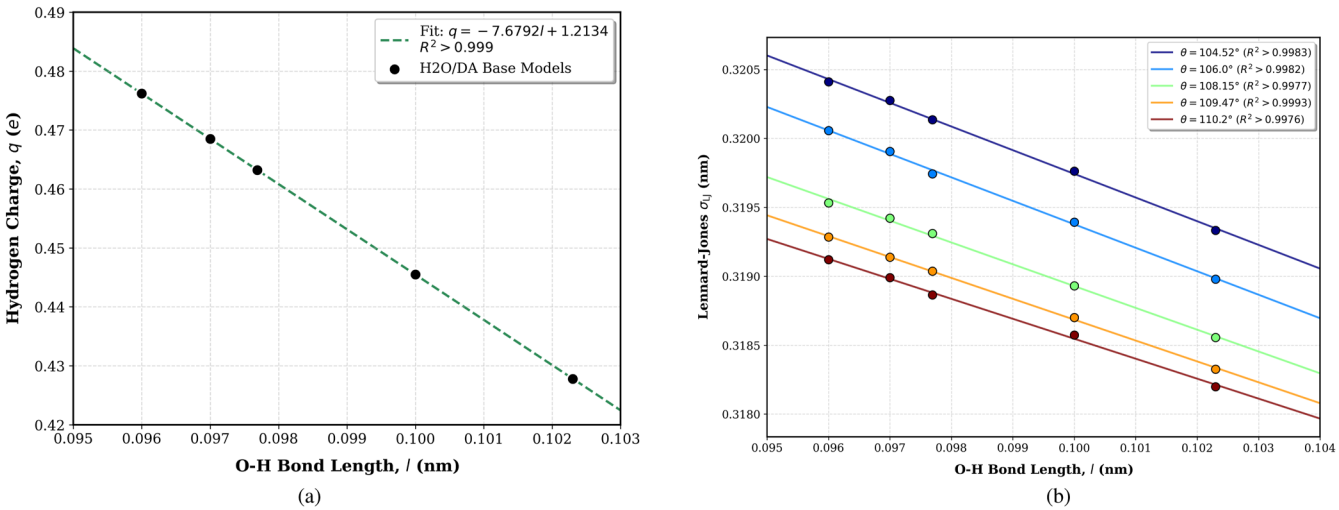

FIG. 2. Scaling laws defining the H_2O/DA manifold. (a) Universal charge scaling $q(l)$, showing the optimal partial charge vs bond length. The inset presents the linear equation relating the optimum charge, q, to the O–H length, l. (b) Angle-dependent steric scaling $\sigma_{LJ}(l,\theta)$. The optimal Lennard-Jones σ varies linearly with length, modulated by the bond angle, serving to calibrate the molecular excluded volume to match the absolute experimental density.

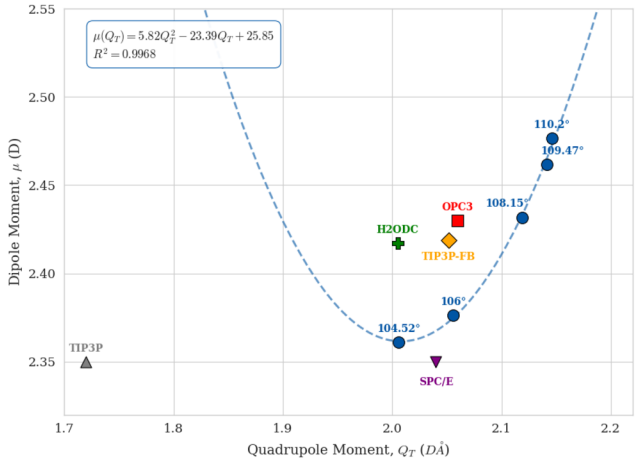

FIG. 4. Electrostatic master curve governing the H_2O/DA_ϵ subset. The blue circles represent our models; the dashed line is the polynomial fit [Eq. (6)]. The state-of-the-art models (OPC3 and H2ODC) cluster near the curve's minimum, confirming this trajectory as a topological boundary (here, topology is used in the physical sense of connectivity and the constraint structure of the parameter space) for accurate rigid water models.

subset represents the rigorous intersection where both the density anomaly and dielectric response are mathematically satisfied.

The members of this H_2O/DA_ϵ subset govern a strict trajectory in the electrostatic phase space, described by a *master curve*, relating the dipole moment (μ) to the quadrupole moment (Q_T),

$$\mu(Q_T) \approx 5.82Q_T^2 - 23.39Q_T + 25.85 \quad (R^2 \approx 0.997). \tag{6}$$

As shown in Fig. 4, this polynomial acts as a physical baseline. Successful empirical models such as OPC3 and TIP3P-FB cluster near the minimum of this curve ($\theta \approx 104.52°$), while classical models such as TIP3P deviate significantly.

Crucially, while Eq. (6) defines the necessary electrostatic balance for dielectric consistency, it does not guarantee thermodynamic stability across all angles. It is precisely the strict adherence to this master curve that forces the system into the geometric incompatibility described in Sec. III C.

C. The geometric–electrostatic no-go condition

The superposition of the density manifold (Sec. III A) and the dielectric master curve creates a fundamental boundary in the parameter space. While high-angle models ($\theta \geq 108°$) successfully

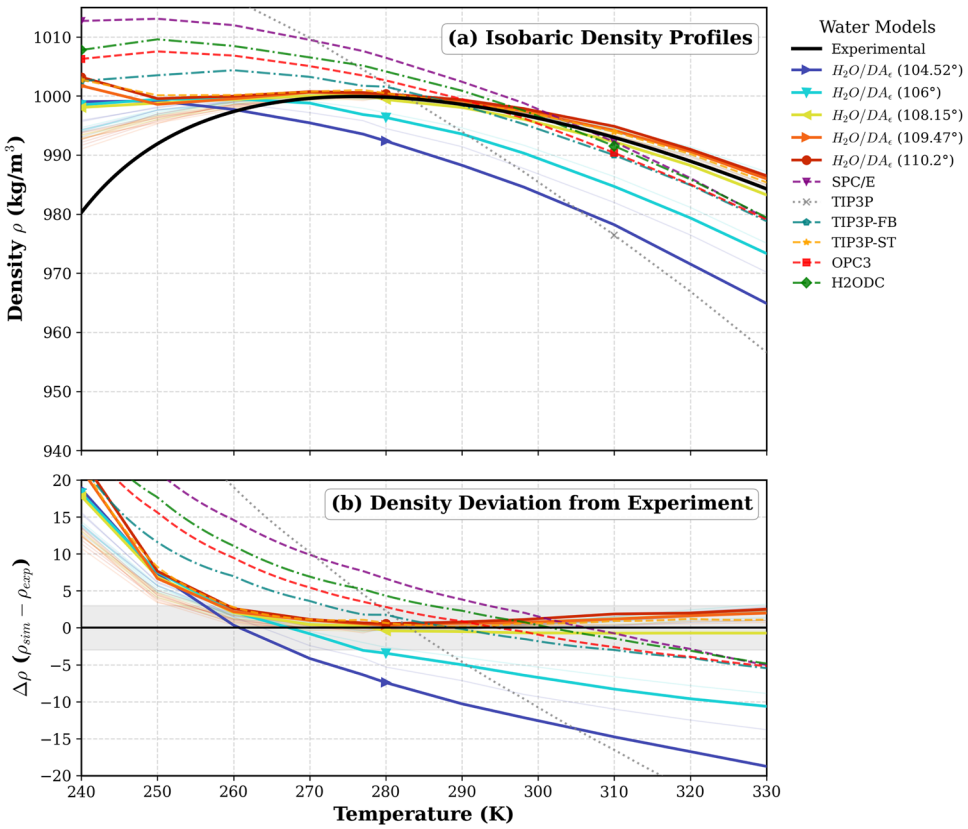

FIG. 5. Thermodynamic consistency and the no-go boundary. The solid lines highlight the ε-optimized models. Note that for $\theta < 108°$, the bond elongation required for dielectric consistency flattens the density curve, shifting the TMD to lower temperatures and degrading α_P. (a) Isobaric density profiles. (b) Density deviation from the experiment.

capture the behavior of water, a distinct physical limit emerges for narrower geometries ($\theta < 107°$).

In this regime, matching the experimental dielectric constant ($\varepsilon \approx 78$) requires a systematic elongation of the O–H bond ($l > 0.105$ nm). However, our sensitivity analysis [Fig. 6(b)] reveals a critical trade-off: the temperature of maximum density exhibits a sharp, inverse dependence on bond length ($T_{MD} \propto -l$). As l increases, the effective volume of the molecule expands,

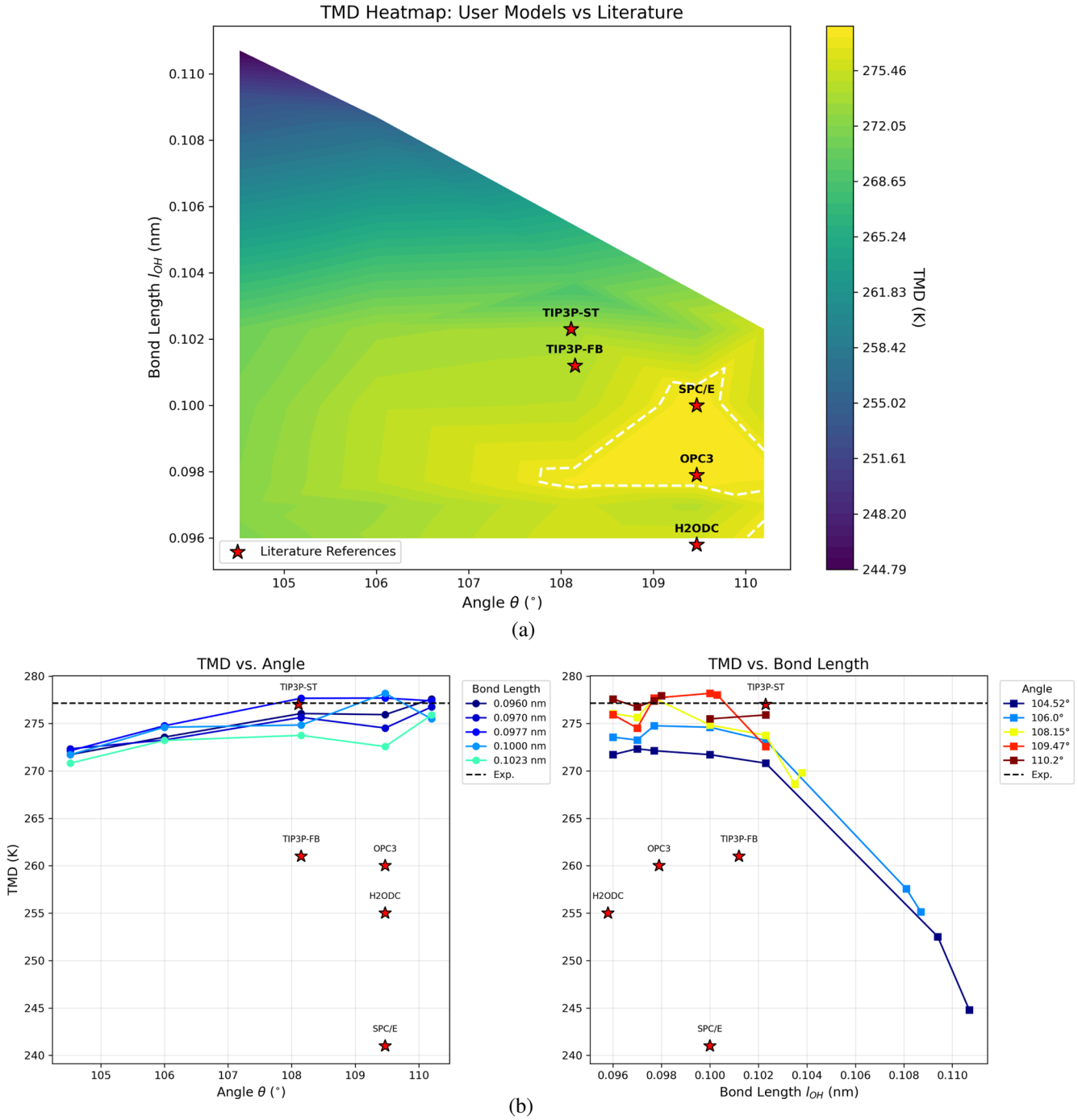

FIG. 6. (a) The TMD error landscape shows that the established models lie outside the optimal zone. (b) Sensitivity analysis reveals the mechanism of the no-go condition: the TMD drops sharply as the bond length l increases, making it impossible to sustain the anomaly at the extended lengths required for dielectric accuracy at low angles.

weakening the tetrahedral network stability required for the anomaly.

Consequently, the very mechanism used to correct the electrostatics (bond elongation) is responsible for destroying the thermodynamics. This is explicitly demonstrated in Fig. 5: for the experimental angle of 104.52°, the elongation required to match ε suppresses the density anomaly entirely, resulting in a flattened isobaric profile without a defined TMD.

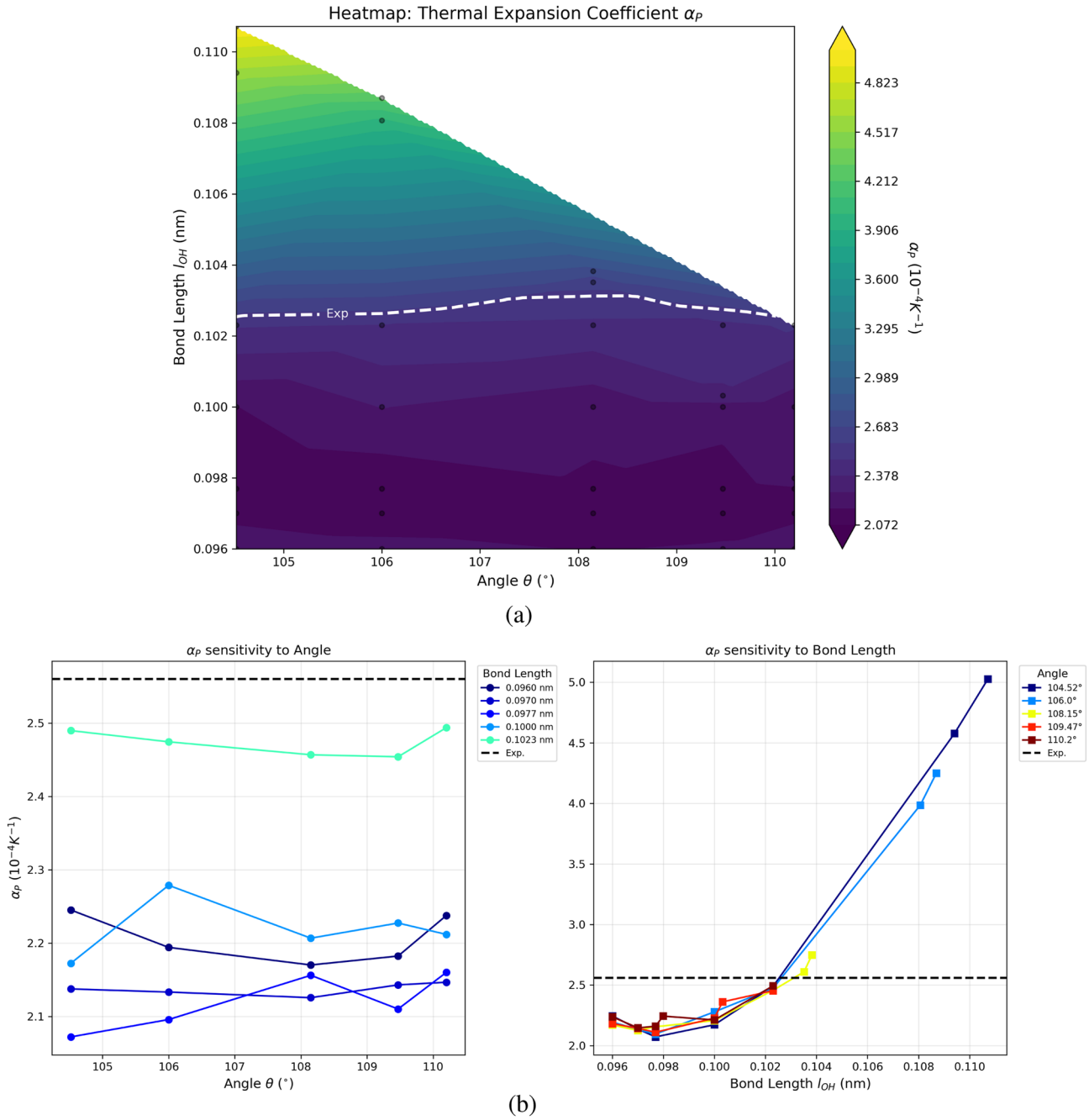

FIG. 7. (a) Heatmap of α_P. The valley of optimal α_P closely follows the density anomaly manifold. (b) Sensitivity analysis shows that α_P is dominated by the bond length, confirming the structural mechanism of the anomaly.

This causal link establishes the first **no-go condition** for rigid three-point models: *it is effectively impossible to simultaneously reproduce the experimental bond angle, the TMD, and the static dielectric constant, because the bond length required for the latter structurally precludes the former.*

This topological barrier rationalizes the historical evolution of water models. Successful parameterizations such as TIP3P-FB and OPC3 have systematically converged toward wider angles (108°–110°). Our analysis confirms that this is not merely an empirical fitting choice, but a necessary condition to access the phase space region, where the dielectric requirement does not force the bond length into a regime that obliterates the density anomaly.

The topology of this limitation is further mapped in Fig. 6. The heatmap of the TMD error reveals a sharp penalty for deviating from the optimal geometric manifold. Furthermore, the sensitivity plots confirm that l is the primary control parameter for the anomaly temperature. The breakdown of linearity at large l (required for low-angle dielectric correction) marks the physical limit, where the rigid three-point approximation fails due to non-linear steric–electrostatic coupling.

It might be hypothesized that increasing the Lennard-Jones potential depth (ε_{LJ}) could stabilize the hydrogen bond network against the disruption caused by bond elongation. However, increasing ε_{LJ} increases the fluid density; the subsequent correction of density requires a larger collision diameter (σ_{LJ}), which effectively negates any stabilization of the TMD or a reduction in the required bond elongation.

TABLE I. Thermal expansion coefficient (α_P) at 298.15 K. The values for the TMD-consistent models ($\theta \geq 108°$) fall within the experimental range, whereas literature models that violate the density manifold to fix electrostatics (e.g., OPC3 and TIP3P-FB) exhibit large errors (>60%). Note that our low-angle models ($\theta < 108°$), discussed in Sec. III F, also exhibit large deviations ($\alpha_P > 4.0$), confirming the no-go limitation.

Model	α_P (10^{-4} K^{-1})	Error (%)
H_2O/*DA* (TMD-consistent)	2.45–2.61	<±4.5
TIP3P-ST	2.40	−6.3
TIP3P-FB	4.10	+60.2
OPC3	4.30	+68.0
H2ODC	4.48	+75.0
TIP3P	9.20	+259.4
SPC/E	5.00	+95.3

D. Thermal expansion as a structural probe

The thermal expansion coefficient (α_P) serves as a strict consistency check for the density anomaly. Since the TMD is mathematically defined by the condition $\alpha_P = 0$, correctly capturing the temperature response of the hydrogen bond network implies that the region of optimal α_P must coincide with the TMD manifold.

Figure 7 confirms this strict physical coupling. The parameter region that minimizes the error in α_P (the "valley of optimality") overlaps precisely with the density-consistent manifold identified in Sec. III A. This demonstrates that the accurate volumetric response is

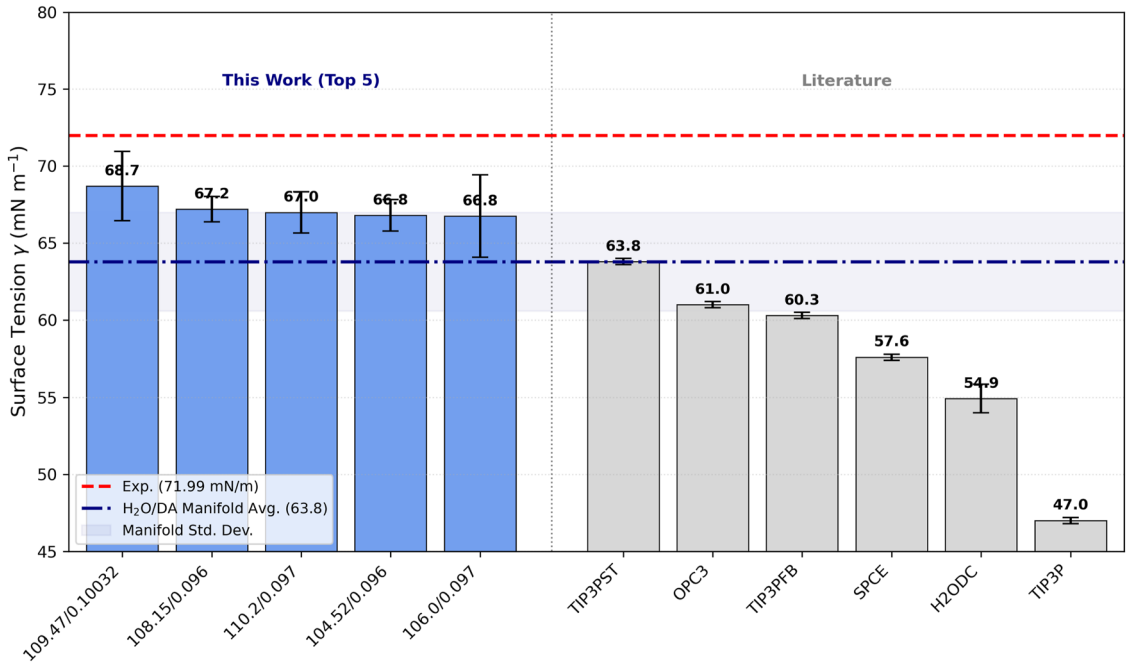

FIG. 8. Surface tension serves as a proxy for structural cohesion. The H_2O/*DA* models (blue) recover high γ values purely from the density constraint, contrasting with standard potentials (gray) that lack the necessary network rigidity.

not an independent parameter to be fitted, but an emergent property of maintaining the correct steric–electrostatic balance.

This coupling further exposes the consequences of the geometric–electrostatic no-go condition. Literature models that prioritize dielectric accuracy at non-tetrahedral angles (e.g., TIP3P-FB and OPC3) are forced out of this optimal manifold. Consequently, as shown in Table I, they systematically overestimate α_P by ~60%–75%.[2,3] In contrast, by strictly adhering to the density manifold, the H_2O/DA family naturally reproduces α_P within 4.5% of the experimental value, without explicit fitting.

The geometric sensitivity analysis [Fig. 7(b)] reinforces that the O–H bond length is the dominant control parameter.[1] High accuracy in α_P requires bond lengths $l_{OH} > 0.102$ nm, suggesting that slight molecular elongation is physically necessary to generate the correct anharmonicity in the rigid three-point potential energy surface.

E. Surface tension as an emergent structural validator

Surface tension (γ) provides a critical probe of the liquid's cohesive energy and local ordering. Within the context of the empirical no-go principles, γ serves as an independent validator of the structural rigidity imposed by the density anomaly constraint.

Figure 8 demonstrates that models belonging to the H_2O/DA manifold naturally reproduce the experimental surface tension as an *emergent property*, without explicit fitting. The average value of 63.8 mN m^{-1} (reaching up to 68.7 mN m^{-1} for optimized geometries) arises directly from the specific electrostatic–steric balance required to stabilize the open tetrahedral network of the density anomaly.

This result highlights a physical dichotomy in rigid three-point modeling. Models that capture the anomalous thermodynamics (H_2O/DA and TIP3P-ST) consistently exhibit high interfacial cohesion. In contrast, models that relax the structural constraints to improve transport properties or simplify parameterization (e.g., standard TIP3P and SPC/E) fail to generate sufficient cohesive force, underestimating γ by up to 35%.

Therefore, high surface tension is identified here not just as a target property, but as the structural signature of a density-consistent model. This strong cohesion, however, acts as the physical precursor to the *thermodynamic–dynamic no-go condition* discussed next: the same rigidity required for realistic interfacial tension inevitably suppresses molecular mobility.

F. Dielectric consistency and the thermodynamic cost

To rigorously probe the fundamental limits of the rigid three-point architecture, we construct the H_2O/DA_ε subset by identifying, for each angular family, the bond length l_{opt} required to reproduce the experimental static dielectric constant ($\varepsilon \approx 78.5$).

As shown in Fig. 9, matching the dielectric constant is mathematically attainable across the entire geometric spectrum. This result highlights that dielectric accuracy alone does not constitute a discriminating criterion for model realism. However, enforcing this constraint carries a nontrivial thermodynamic cost that depends critically on molecular geometry.

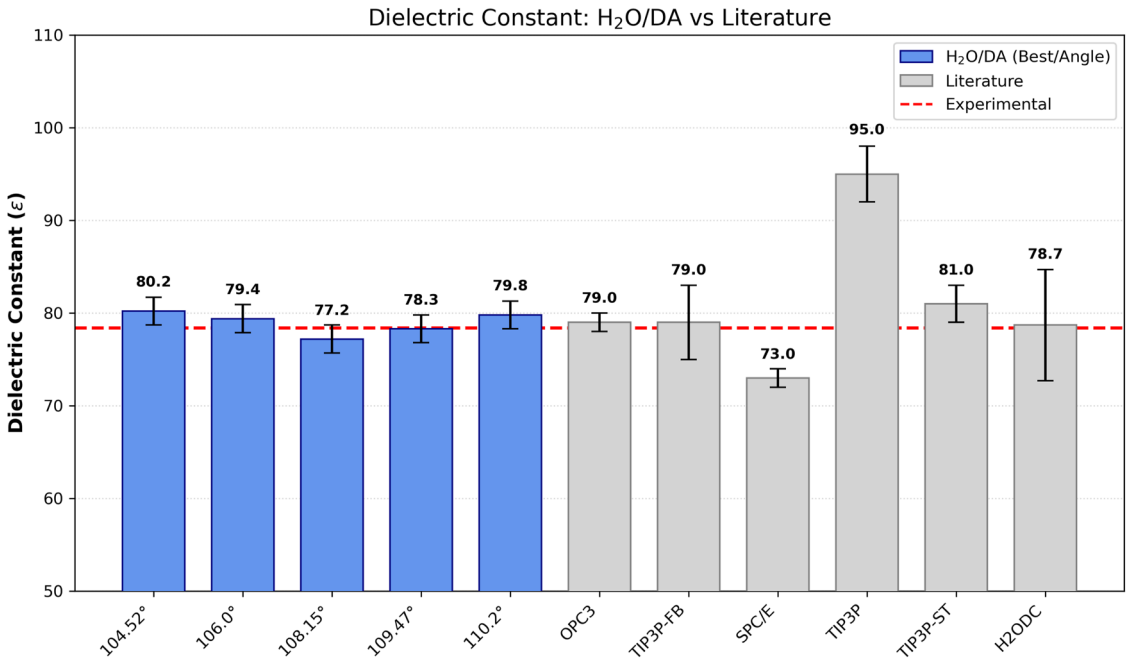

FIG. 9. Static dielectric constant (ε) as a function of molecular geometry. While ε can be reproduced at any bond angle, only high-angle geometries do so without violating thermodynamic consistency. The blue bars represent the H_2O/DA_ε family models, and the gray bars denote the literature values taken from Refs. 4 and 15.

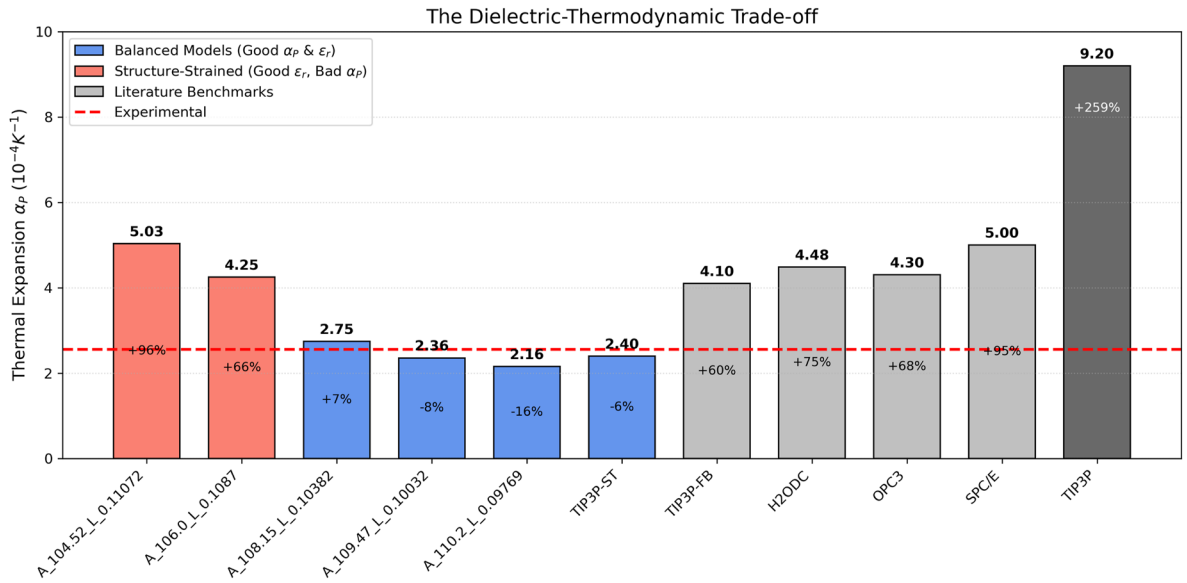

FIG. 10. Thermodynamic cost of enforcing dielectric consistency. Models that reproduce ε at low bond angles (red bars, e.g., OPC3) severely overestimate the thermal expansion coefficient, effectively destroying the density anomaly. In contrast, only high-angle geometries (blue bars) simultaneously satisfy both dielectric and thermodynamic constraints. The literature values were taken from Refs. 4 and 15.

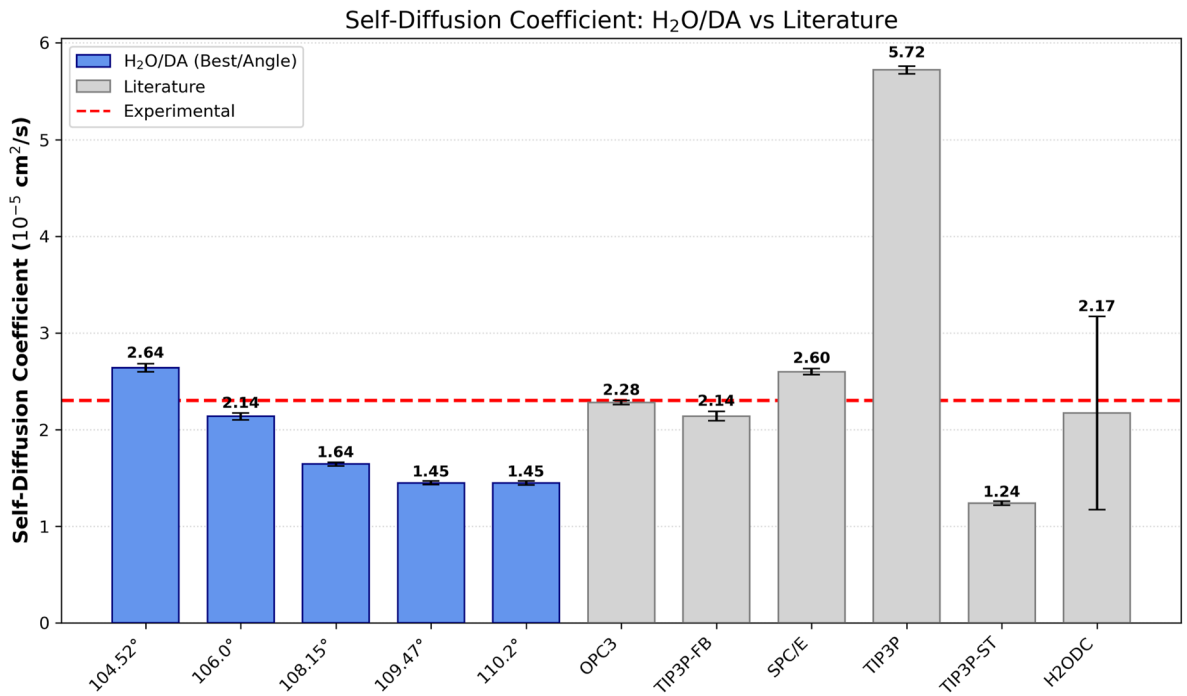

FIG. 11. Kinetic penalty of thermodynamic consistency. Comparison of self-diffusion coefficients (D) between the density-consistent H_2O/DA_ε models (blue) and standard literature models (gray)[4,15] at 298.15 K. The dashed line represents the experimental value (2.30×10^{-5} cm^2 s^{-1}). While literature models such as OPC3 achieve experimental mobility, they do so by violating the steric constraints required for the density anomaly. In contrast, models confined to the TMD manifold systematically underestimate D, illustrating the thermodynamic–dynamic no-go condition. Error bars represent the standard error of the mean.

This cost is revealed by the dielectric–thermodynamic trade-off shown in Fig. 9. For water-like, narrow geometries (104.52°–106.00°), the bond elongation required to reproduce ε leads to a severe overestimation of the thermal expansion coefficient, with $\alpha_P > 4.0 \times 10^{-4}$ K^{-1}. As a consequence, the temperature of maximum density is either shifted far from its experimental value or completely lost.

This behavior mirrors that of modern rigid three-point potentials, such as OPC3 and H2ODC, which accurately reproduce ε but systematically fail to describe α_P, with errors exceeding 60%. Within the present framework, this failure is not incidental but constitutes direct evidence of a *geometric–electrostatic no-go condition*: for experimental bond angles, dielectric consistency and thermodynamic consistency are mutually incompatible in rigid three-point models (Fig. 10).

In contrast, geometries approaching the tetrahedral limit ($\theta \approx 109.47°$) evade this incompatibility. In this regime, the bond length required to reproduce ε remains compatible with the density-anomaly manifold, allowing α_P to be simultaneously reproduced within acceptable accuracy. This behavior rationalizes the high-angle strategy implicitly adopted by models such as TIP3P-ST and confirms that tetrahedral geometries represent the only thermodynamically admissible solution for dielectric consistency within the rigid three-point framework.

G. Dynamics as a consequence of structural optimality

While tetrahedral H_2O/DA models resolve the dielectric–thermodynamic incompatibility, they expose a second, independent limitation associated with molecular transport. The self-diffusion coefficients obtained for these structurally consistent models lie in the range $D \approx (1.4-1.6) \times 10^{-5}$ cm^2 s^{-1}, systematically below the experimental value of $\approx 2.3 \times 10^{-5}$ cm^2 s^{-1} (Fig. 11).

This reduction in mobility is not a failure of parameterization but a direct structural consequence of enforcing the density anomaly. The enhanced rigidity of the hydrogen-bond network required to stabilize the tetrahedral arrangement necessarily suppresses translational motion. Within the present framework, this establishes the *thermodynamic–dynamic no-go condition*: the simultaneous reproduction of the temperature of maximum density and the experimental self-diffusion coefficient is unattainable within rigid three-point models.

Together, these results demonstrate that dielectric accuracy, thermodynamic anomalies, and molecular mobility cannot be jointly optimized within a rigid three-site architecture. The observed trade-offs are, therefore, intrinsic, delineating the fundamental boundaries of this model class.

H. Compressibility and diffusion: Structural trade-offs

While the H_2O/DA models accurately reproduce the liquid density, the thermal expansion coefficient, and—through the master-curve extrapolation—the static dielectric constant, the second-order thermodynamic and dynamical properties exhibit systematic deviations. These behaviors are not numerical artifacts, but rather intrinsic physical consequences of imposing strict density-anomaly constraints within a rigid three-site framework.

For the isothermal compressibility, the computed values across all 34 models lie within a narrow interval of $\kappa_T \in [4.15, 4.35] \times 10^{-10}$ Pa^{-1}. A comparison with the experimental value at 298 K ($\kappa_T^{\mathrm{exp}} \approx 4.6 \times 10^{-10}$ Pa^{-1}) reveals a consistent underestimation, indicating that the optimized equation of state is slightly too stiff. The weak dependence of κ_T on either bond length l or angle θ suggests that once the density and the TMD are enforced, the magnitude of volumetric fluctuations becomes effectively predetermined. This coupling between the density constraint and the repulsive-core stiffness is a known limitation of rigid three-point models, shared by parameterizations such as OPC3 and TIP3P-FB.

A more pronounced structural signature arises in the self-diffusion coefficient (D) 11. The H_2O/DA family yields values in the range $D \in [1.08, 1.30] \times 10^{-5}$ cm^2 s^{-1}, significantly below the experimental expectation ($D_{\mathrm{exp}} \approx 2.30 \times 10^{-5}$ cm^2 s^{-1}). Despite this systematic deviation, internal trends across the manifold remain physically consistent: for a fixed angle, increasing the bond length l correlates with an increase in D. For instance, at $\theta = 104.52°$, increasing l from 0.096 to 0.1 nm raises the diffusion coefficient from 1.09 to 1.24×10^{-5} cm^2 s^{-1}. This trend parallels the linear dielectric scaling described in Sec. III B, indicating that geometric tuning, which enhances the dipole moment, also modifies the rigidity of the local hydration cage, modestly facilitating molecular mobility.

That the diffusion coefficient remains systematically lower than the experiment reflects a fundamental topological trade-off. Achieving realistic density and TMD behavior in rigid three-point models requires a structurally reinforced hydrogen-bond network that inevitably suppresses translational mobility. Consequently, the simultaneous optimization of first-order thermodynamic properties (density, TMD, α_P) and dynamical properties (diffusion) is intrinsically limited. The H_2O/DA manifold prioritizes structural and thermodynamic fidelity, accepting slower dynamics as the necessary and physically consistent consequence of strictly reproducing the density anomaly.

I. The Pareto frontier: A structural–dynamic bifurcation

The synthesis of our geometric and dynamic analyses reveals that the limitations of rigid three-point water models are not methodological, but topological. As visualized in the global error landscape (Fig. 12), there exists a fundamental *Pareto frontier*, where thermodynamic fidelity and transport rates compete.

This landscape exposes a distinct bifurcation in model design:

- The **dynamics-first branch** (e.g., OPC3 and TIP3P-FB): These models occupy the upper-left region. They achieve experimental diffusion rates (D) and dielectric constants (ε) by relaxing the tetrahedral stiffness. Consequently, models optimized for ambient density (such as OPC3) serve biomolecular applications excellently, where solvation and mobility at physiological temperatures are paramount. However, the inevitable cost, as predicted by the first no-go theorem, is the degradation of the density anomaly and thermal expansion (α_P errors >60%).
- The **structure-first branch** (H_2O/DA and TIP3P-ST): These models occupy the lower-right region. By prioritizing the density anomaly, they naturally recover surface tension and

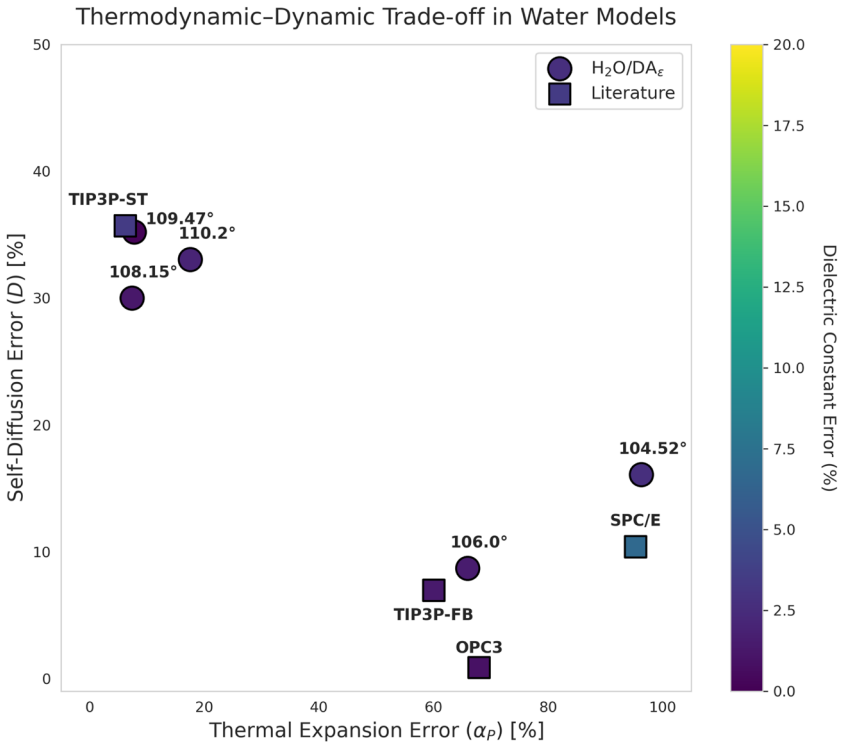

FIG. 12. Pareto frontier of rigid three-point water models. The scatterplot reveals the intrinsic bifurcation: one can minimize the structural error (α_P, left) or the dynamic error (D, top), but not both simultaneously. The color scale indicates the ε error. Our H_2O/DA models (circles) prioritize the structural branch, accepting slower dynamics to preserve the density anomaly, while literature models (squares) sacrifice the anomaly for speed.

heat capacity. However, as predicted by the second empirical no-go principle, the structural rigidity required for these properties imposes a kinetic penalty, reducing diffusion by ~20 – 30%.

This trade-off is physically intrinsic. The "structural tightening" observed in the oxygen–oxygen radial distribution function (g^1_{OO}) for H_2O/DA models confirms that the very cage rigidity needed to stabilize the TMD is what restricts molecular mobility.

TABLE II. Global performance comparison at 298.15 K. Errors are reported as Absolute Percentage Error (APE) relative to experimental references. The global score (ξ_{global}) is the unweighted average APE over all eight properties. Bold values indicate the minimum error (best performance), and italic values indicate the maximum error (worst performance) for each property across all models. Experimental values: ρ = 997 kg m^{-3}, ΔH_{vap} = 44.0 kJ mol^{-1}, α_P = 2.6 × 10^{-4} K^{-1}, κ_T = 45.2 × 10^{-6} bar^{-1}, ε = 78.4, γ = 72.0 mN m^{-1}, D = 2.3 × 10^{-5} cm^2 s^{-1}, C_p = 75.3 J mol^{-1} K^{-1}.

Model	ρ	ΔH_{vap}	α_P	κ_T	ε	γ	D	C_p	ξ_{global}
Classical									
TIP3P	*1.7*	0.5	*259.4*	2.1	*21.2*	*34.7*	*148.7*	*11.2*	*59.9*
SPC/E	0.3	0.9	95.3	1.8	6.9	21.0	10.4	**1.2**	17.2
Modern									
TIP3P-FB	0.7	2.2	60.2	5.2	0.8	16.3	7.0	5.6	12.3
OPC3	0.6	0.5	68.0	2.5	0.8	15.3	**0.9**	4.1	11.6
H2ODC	0.1	1.4	75.0	**0.7**	0.4	23.7	5.7	3.3	13.8
TIP3P-ST	0.1	*7.8*	**6.7**	*12.3*	3.3	11.4	35.4	4.9	10.2
This work									
A_109.47_L_0.10 032	**0.0**	3.4	7.8	5.1	**0.0**	**4.6**	34.2	2.8	**7.2**
A_108.15_L_0.10 382	0.1	**0.3**	7.3	3.0	1.4	13.7	29.4	3.1	7.3

Therefore, the H_2O/DA manifold represents a conscious choice for the structural branch. We posit that for applications where phase behavior, interfacial thermodynamics, and structural ordering are paramount, the underestimation of diffusion is an acceptable and physically consistent price to pay for retaining the density anomaly.

J. Minimizing the error under no-go constraints

The no-go conditions established in Secs. III A–III I imply that a "perfect" rigid three-point water model is topologically impossible. Consequently, the goal shifts from seeking an unattainable ideal to identifying the **optimal physical compromise**.

To quantify this, we define a global performance score (ξ_{global}) based on the Mean Absolute Percentage Error (MAPE) over eight diverse physical properties. This metric treats all observables equally, allowing us to evaluate which strategy—prioritizing structure or dynamics—yields the best average representation of liquid water.

Table II presents the results, revealing a distinct hierarchy and bifurcation in model design:

1. **The classical baseline (TIP3P and SPC/E):** These early models suffer from large deviations. TIP3P, in particular, exhibits massive errors in expansion (α_P) and dynamics, yielding a global error score of ~58%.
2. **The dynamic branch (OPC3 and TIP3P-FB):** These modern potentials minimize diffusion errors (D error <1%) and dielectric deviations. However, as predicted by the first empirical no-go principle, this comes at a severe cost to structural derivatives (α_P errors >24 – 60%) and surface tension, resulting in global scores between 7.8% and 11.6%.
3. **The structural branch (TIP3P-ST and H_2O/DA):** The TIP3P-ST model, which like our work prioritizes surface tension and density, confirms the physical trade-off: it achieves excellent α_P accuracy (6.7% error) but suffers from slow dynamics (35% error in D).

Our H_2O/DA framework refines this "structural strategy." By strictly adhering to the density manifold, our models achieve the lowest global error scores in this study ($\xi_{global} \approx 7.2\%$). They outperform the "dynamic strategy" of TIP3P-FB and OPC3 on average, demonstrating that while the kinetic penalty is unavoidable in rigid models, it is numerically smaller than the structural distortions required to fix the dynamics.

Notably, our tetrahedral model (A_109.47_L_0.10032) surpasses TIP3P-ST (ξ = 10.2%) by improving the enthalpy of vaporization and dielectric constant, offering the most balanced rigid three-point representation currently available for thermodynamic and interfacial applications.

K. Generalization: The hierarchy of anomalous constraints

The findings of this work suggest a broader theoretical implication. We posit that the density anomaly is not unique in its organizing role; rather, it is likely the most accessible member of a broader *hierarchy of water anomalies*, each imposing independent topological constraints on the admissible parameter space.

Just as the density anomaly confines the parameter space to the H_2O/DA manifold, we hypothesize that other anomalous behaviors, such as the diffusivity anomaly (maximum in D under pressure) or the heat capacity anomaly, define their own characteristic manifolds. In this geometric framework, the "perfect" water model would correspond to the mutual intersection of all these anomalous surfaces.

However, the empirical no-go principles identified here for the density anomaly imply that these manifolds may not necessarily overlap within the rigid three-point architecture. For instance, the region of parameter space that satisfies the structural anomaly (TMD) is shown here to be topologically distinct from the region satisfying fast dynamics. This suggests that the phase space of rigid water models is fragmented, preventing the simultaneous capture of the full hierarchy of water's anomalous physics.

Furthermore, the framework could be extended to explore the thermodynamic stability of water in the supercooled regime. By incorporating the relative free energy between the liquid and ice as an additional constraint, one could define a "low-temperature optimality sub-manifold." However, consistent with the no-go principles identified here, we anticipate that enforcing the experimental melting point within a rigid three-point architecture would likely displace the density anomaly toward higher temperatures. This potential incompatibility reinforces our thesis that the parameter space is fragmented, preventing a simultaneous and accurate capture of the full hierarchy of water's anomalous physics.

This perspective recasts the future of water modeling: the challenge is not merely to "fit" parameters, but to map the topology of these intersecting (or disjoint) manifolds. Understanding which anomalies are topologically compatible and which are mutually exclusive will be key to designing next-generation purpose-specific force fields.

IV. CONCLUSION

In this work, rather than proposing a standard parameter optimization, we investigated the topological limits of the rigid three-point water model architecture. By elevating the density anomaly to a master holonomic constraint, we demonstrated that physically meaningful models collapse onto a low-dimensional *manifold of optimality* (H_2O/DA).

Our analysis suggests that the failure of three-point models to simultaneously reproduce thermodynamic and dynamic anomalies arises not only from incomplete parameter optimization, but also from fundamental physical constraints that govern the admissible parameter space. Consequently, instead of introducing yet another parameterization, we establish a unifying physical framework explaining why certain combinations of thermodynamic, dielectric, and dynamical properties are intrinsically unattainable within this architecture. Along this manifold, electrostatic strength, steric repulsion, and molecular geometry are deterministically coupled through robust scaling relations, transforming model development from a high-dimensional empirical search into a problem of navigation along physically admissible trajectories.

This topology exposes the fundamental boundaries of the rigid three-point approximation, formalized here as two *empirical no-go principles*. First, a *geometric–electrostatic incompatibility* prohibits the simultaneous reproduction of the experimental bond angle, the

temperature of maximum density, and the static dielectric constant. Second, a *thermodynamic–dynamic limitation* establishes that the structural rigidity required to stabilize the density anomaly necessarily suppresses molecular mobility, rendering the experimental diffusion coefficient unattainable. Together, these constraints define a Pareto frontier, where thermodynamic fidelity and transport properties are mutually exclusive.

These limitations are, therefore, intrinsic architectural features, not artifacts of parameterization strategy. The role of rigid three-point models must accordingly be redefined: not as universal representations of liquid water but as purpose-driven approximations, whose applicability is inherently conditional. Within this perspective, the performance of the established parameterizations should be interpreted as explicit choices along a constrained trade-off surface. Models such as OPC3 prioritize the dynamic branch, while the H_2O/DA family occupies the structural branch, emphasizing phase behavior and thermodynamic consistency.

The framework introduced here provides a transparent and predictive basis for making such choices and for guiding the systematic design of force fields tailored to specific applications. While the present analysis focused on a fixed dispersion depth, extensions to variable energetic parameters may generalize the manifold to a broader hyperspace. Nevertheless, the topological constraints identified in this work are expected to remain invariant, defining the fundamental physical limits of the rigid three-point architecture.

ACKNOWLEDGMENTS

The authors acknowledge the National Council for Scientific and Technological Development (CNPq) (Grant No. 311707/2021-1) for financial support.

AUTHOR DECLARATIONS

Conflict of Interest

The authors have no conflicts to disclose.

Author Contributions

Jefferson Santana Martins: Conceptualization (equal); Data curation (equal); Formal analysis (equal); Writing – original draft (equal); Writing – review & editing (equal). **Raúl Fuentes-Azcatl**: Conceptualization (equal); Writing – review & editing (equal). **Marcia C. Barbosa**: Conceptualization (equal); Supervision (equal); Writing – original draft (equal).

DATA AVAILABILITY

The data that support the findings of this study are available from the corresponding author upon reasonable request.

REFERENCES

[1] J. S. Martins, R. Fuentes-Azcatl, and M. C. Barbosa, J. Phys.: Condens. Matter **37**, 455101 (2025).
[2] L.-P. Wang, T. J. Martinez, and V. S. Pande, J. Phys. Chem. Lett. **5**, 1885 (2014).
[3] S. Izadi and A. V. Onufriev, J. Chem. Phys. **145**, 074501 (2016).
[4] C. J. Fennell, L. Li, and K. A. Dill, J. Phys. Chem. B **116**, 6936 (2012).
[5] C. Vega, J. L. F. Abascal, E. Sanz, L. G. MacDowell, and C. McBride, J. Phys.: Condens. Matter **17**, S3283 (2005).
[6] Y. Qiu, P. S. Nerenberg, T. Head-Gordon, and L.-P. Wang, J. Phys. Chem. B **123**, 7061 (2019).
[7] M. W. Mahoney and W. L. Jorgensen, J. Chem. Phys. **112**, 8910 (2000).
[8] S. Izadi, B. Aguilar, and A. V. Onufriev, J. Chem. Theory Comput. **11**, 4450 (2015).
[9] H. J. Berendsen, J. P. Postma, W. F. van Gunsteren, and J. Hermans, in *Intermolecular Forces: Proceedings of the Fourteenth Jerusalem Symposium on Quantum Chemistry and Biochemistry Held in Jerusalem, Israel, April 13–16, 1981* (Springer, 1981), pp. 331–342.
[10] H. J. C. Berendsen, J. R. Grigera, and T. P. Straatsma, J. Phys. Chem. **91**, 6269 (1987).
[11] W. L. Jorgensen *et al.*, J. Chem. Phys. **79**, 926 (1983).
[12] G. S. Kell, J. Chem. Eng. Data **20**, 97 (1975).
[13] C. Vega, M. M. Conde, C. McBride, J. L. F. Abascal, E. G. Noya, R. Ramírez, and L. M. Sesé, J. Chem. Phys. **132**, 046101 (2010).
[14] I.-C. Yeh and G. Hummer, J. Phys. Chem. B **108**, 15873 (2004).
[15] S. P. Kadaoluwa Pathirannahalage, N. Meftahi, A. Elbourne, A. C. G. Weiss, C. F. McConville, A. Padua, D. A. Winkler, M. Costa Gomes, T. L. Greaves, T. C. Le *et al.*, J. Chem. Inf. Model. **61**, 4521 (2021).